

The origin of complex organic molecules in prestellar cores

C. Vastel^{1,2}

Université de Toulouse, UPS-OMP, IRAP, Toulouse, France

CNRS, IRAP, 9 Av. colonel Roche, BP 44346, 31028 Toulouse Cedex 4, France

`cvastel@irap.omp.eu`

C. Ceccarelli^{3,4} and B. Lefloch^{3,4}

Univ. Grenoble Alpes, IPAG, F-38000 Grenoble, France

CNRS, IPAG, F-38000 Grenoble, France

R. Bachiller⁴

Observatorio Astronómico Nacional (OAN, IGN). Calle Alfonso XII,3. 28014 Madrid, Spain

Received - ; accepted -

ABSTRACT

Complex organic molecules (COMs) have been detected in a variety of environments, including cold prestellar cores. Given the low temperature of these objects, these last detections challenge existing models. We report here new observations towards the prestellar core L1544. They are based on an unbiased spectral survey of the 3mm band at the IRAM-30m telescope, as part of the Large Program ASAI. The observations allow us to provide the full census of the oxygen bearing COMs in this source. We detected tricarbon monoxide, methanol, acetaldehyde, formic acid, ketene, and propyne with abundances varying from 5×10^{-11} to 6×10^{-9} . The non-LTE analysis of the methanol lines shows that they are likely emitted at the border of the core, at a radius of ~ 8000 AU where $T \sim 10$ K and $n_{H_2} \sim 2 \times 10^4 \text{ cm}^{-3}$. Previous works have shown that water vapour is enhanced in the same region because of the photodesorption of water ices. We propose that a non-thermal desorption mechanism is also responsible for the observed emission of methanol and COMs from the same layer. The desorbed oxygen and a tiny amount of desorbed methanol and ethene are enough to reproduce the abundances of tricarbon monoxide, methanol, acetaldehyde and ketene measured in L1544. These new findings open the possibility that COMs in prestellar cores originate in a similar outer layer rather than in the dense inner cores, as previously assumed, and that their formation is driven by the non-thermally desorbed species.

Subject headings: astrochemistry—line: identification—ISM: abundances—ISM: molecules—ISM: individual objects (L1544)

1. Introduction

Interstellar complex organic molecules (hereinafter COMs) are defined in the astrochemical literature as organic molecules containing at least six heavy atoms (Herbst & van Dishoeck 2009). Among the discovered interstellar molecules, COMs are of particular interest for their potential relation with the origin of the terrestrial life and, more prosaically, because they are a powerful diagnostic to understand the matter chemical evolution during the formation of planetary systems like our own (Caselli & Ceccarelli 2012).

COMs were first detected in the hot cores associated with high-mass star forming regions (Cummins et al. 1986; Blake et al. 1986). Since then, they have been discovered in a variety of environments such as low-mass hot corinos (Cazaux et al. 2003; Bottinelli et al. 2004; Ceccarelli 2005) and cold envelopes (Jaber et al. 2014), Galactic Center cold clouds (Requena-Torrelles et al. 2006), and prestellar cores (Öberg et al. 2010; Cernicharo et al. 2012; Bacmann et al. 2012).

Currently, models predict that (most of) COMs are synthesised on the interstellar grain surfaces when they warm up at temperatures ≥ 30 K, thanks to the enhanced mobility of heavy elements and radicals on the surface (e.g. Garrod & Herbst 2006; Garrod et al. 2009). The detection of COMs in cold (≤ 20 K) environments represents a challenge to those models because the mentioned mechanism cannot work at those temperatures. Besides, the process that releases iced species from the grain surfaces into the gas phase is a problematic issue at such low temperatures. Recently, Vasyunin & Herbst (2013) proposed a mechanism, that they call reactive desorption, in which the exothermicity of surface chemical reactions make the species to be desorbed after their formation. Assuming an ejection efficiency of 10%, this model can approximatively reproduce the abundances observed in prestellar cores of dimethyl ether (CH_3OCH_3), acetaldehyde (CH_3CHO), ketene (H_2CCO) and methanol (CH_3OH), but it fails to reproduce other species such as formaldehyde (H_2CO), methyl formate (HCOOCH_3) and methoxy (CH_3O).

Given the key role that the presence of COMs in prestellar cores has in understanding the general mechanisms of their formation, it is of paramount importance (i) to have a as complete as possible census of the COMs present in prestellar cores, (ii) to better characterise where the COMs emission comes from in these cold objects and, as a consequence, (iii) to have a better determination of their abundance, at present obtained by dividing the measured species column density by the total H_2 column density of the core.

In this Letter, we present a complete census of the oxygen bearing COMs, and other key species useful to constrain COMs formation processes, in the prestellar core L1544. The census has been obtained by analysing the unbiased spectral survey in the 3mm band carried out at the IRAM-30m telescope, within the Large Programme ASAI (Astrochemical Surveys At Iram)¹.

¹<http://www.oan.es/asai/>

2. The source

L1544 is a prototypical starless core in the Taurus molecular cloud complex ($d \sim 140$ pc) on the verge of the gravitational collapse (Caselli et al. 2002 and references within). It is characterised by a central high density ($2 \times 10^6 \text{ cm}^{-3}$), low temperature (~ 7 K; Crapsi et al. 2007), and high CO depletion, accompanied by a large degree of molecular deuteration (Caselli et al. 2003; Crapsi et al. 2005; Vastel et al. 2006). Its physical and dynamical structure has been recently reconstructed by Caselli et al. (2012; hereinafter CKB2012) and Keto et al. (2014) using the numerous existing observations towards L1544. Among them, we emphasise the recent detection of water vapour by the Herschel Space Observatory, the first water detection ever in a prestellar core, which provided a key information to reconstruct the physical and chemical structure of L1544 (CKB2012). In fact, the observed water line shows an inverse P-Cygni profile, characteristic of gravitational contraction, confirming that L1544 is on the verge of the collapse. Based on the line shape, CKB2012 predict that water is largely frozen into the grain mantles in the interior (≤ 4000 AU) of the L1544 core, where the gaseous H_2O abundance (with respect to H_2) is only $\sim 10^{-9}$. The low but not zero level of water vapour is believed to be caused by the photodesorption of water molecules from the icy mantles by the FUV photons created by the interaction of cosmic rays with H_2 molecules. Farther away from the center ($\sim 10^4$ AU), where the density is low enough ($\leq 10^5 \text{ cm}^{-3}$) for the photodesorption rate not to be overcome by the freeze-out rate, the gaseous H_2O abundance reaches $\sim 3 \times 10^{-7}$, as predicted by previous models (Dominik et al. 2005; Hollenbach et al. 2009).

3. Observations and results

The observations were performed on July 3rd, 2013 and September 10th, 2013 toward L1544 ($\alpha_{2000} = 05^h04^m17.21^s$, $\delta_{2000} = 25^\circ10'42.8''$). Using the 3 mm Eight Mixer Receivers (16 GHz of total instantaneous bandwidth per polarisation) and the fast Fourier Transform Spectrometers with a spectral resolution of 50 kHz (allowing the observation of the inner 1.82 GHz of each band), six set-ups were needed to cover the full band, namely the frequency range between 81–110 GHz. Two higher energy level transitions of the C_3O species, at 96.2 and 105.8 GHz respectively, were observed during the January 2014 run to reach a better rms.

Weather conditions were average with 2 to 3 mm of precipitable water vapour. System temperatures were between 110 and 180 K, resulting in an average rms of 4 to 7 mK in a 50 kHz frequency bin. In order to obtain a flat baseline, observations were carried out using a nutating secondary mirror, with a throw of 3 arcmin. No contamination from the reference position was observed. Pointing was checked every 1.5 hours on the nearby continuum sources 0439+360 and 0528+134. Pointing errors were always within $3''$. We adopted the telescope and receiver parameters (main-beam efficiency, half power beam width, forward efficiency) from the values monitored at IRAM (<http://www.iram.fr>). Line intensities are expressed in units of main-beam brightness

temperature.

We detected several lines from E- and A- CH_3OH and $^{13}\text{CH}_3\text{OH}$, CH_3CHO , t-HCOOH, H_2CCO , E- CH_3CCH , and C_3O . All lines, for the first time detected in L1544, are in emission, except the 107 GHz line of E- CH_3OH , which appears in absorption. We did not detect any other oxygen bearing COM. Important non-detections include CH_3OCH_3 , HCOOCH_3 and CH_3O , which were, on the contrary, detected in other prestellar cores (Öberg et al. 2010; Cernicharo et al. 2012; Bacmann et al. 2012).

Figures 1 and 2 show the detected transitions of C_3O , A- and E- CH_3OH , CH_3CHO , t-HCOOH, H_2CCO , E- CH_3CCH . Using the CASSIS² software, the lines have been fitted using the Levenberg-Marquardt function. The parameters resulting from the fit are listed in Table 1.

4. Derivation of the column densities

We carried out an LTE analysis of the observed line intensities for all the detected species (except CH_3OH , see below). We assumed that the source fills the beam³ and we carried out a rotational diagram analysis for the species in which more than one line has been detected, namely all the detected species except C_3O and t-HCOOH. Specifically, we computed a grid of LTE models for the CH_3CHO , H_2CCO and E- CH_3CCH lines. Then, for each species, we found the best fit parameters varying the linewidth, V_{LSR} , excitation temperature (assumed to be the same in all observed lines) and column density. In the cases of C_3O and t-HCOOH, we adopted an excitation temperature equal to 10 K. The results of this analysis are reported in Table 2.

In the case of CH_3OH , we carried out a non-LTE analysis, considering the A and E forms separately and assuming an abundance ratio 1:1 between them and the $^{12}\text{C}/^{13}\text{C}$ equal to 75. We used the Large Velocity Gradient (LVG) code described in Ceccarelli et al. (2003) and the collisional rates by Rabli & Flower (2010), retrieved from the BASECOL data base (<http://basecol.obspm.fr>; Dubernet et al. 2013). We run a large grid of models varying the methanol column density from 5×10^{12} to $6 \times 10^{13} \text{ cm}^{-2}$, the density from 1×10^4 to $1 \times 10^6 \text{ cm}^{-3}$, the temperature from 7 to 16 K, and the source size from 1'' to 200''. For each methanol column density, we found the source size, temperature and density with the minimum reduced χ^2 . All solutions with reduced $\chi^2 \leq 0.8$ are considered good (equivalent to a probability of 1 σ). With this criterium, we found that CH_3OH column densities between 2.6 to $3.8 \times 10^{13} \text{ cm}^{-2}$ are consistent with the data. The observed lines are optically thick for $N(\text{CH}_3\text{OH}) \geq 3.8 \times 10^{13} \text{ cm}^{-2}$ and this allows us to constrain also the emitting size to be larger than about 30''. At larger sizes, the beam filling factor becomes

²<http://cassis.irap.omp.eu/>

³This is a reasonable assumption based on the numerous previous observations towards L1544. Nonetheless, since the observed lines have frequencies that differ less than 20%, including a possible filling factor does not substantially change the results.

unity and the lines optically thin. The temperature and density are degenerate, as shown in Fig. 3 for the two extreme methanol column densities. Note, however, that the derived density is $\leq 10^5 \text{ cm}^{-3}$ and the temperature is between 7 and 15 K for a density between 10^4 and 10^5 cm^{-3} . Note also that the best fit models correctly reproduce the absorption line at 107 GHz.

Finally, the non-detection of lines from CH_3OCH_3 , HCOOCH_3 and CH_3O provide upper limits to their column density of 1×10^{12} , 6×10^{12} and 6×10^{11} , respectively.

5. Spatial origin and abundances of the COMs

The analysis of the CH_3OH lines provides a strong constraint on the gas density, which has to be $\leq 10^5 \text{ cm}^{-3}$. This means that the bulk of the CH_3OH emission does not originate in the dense interior of the L1544 core, but in a less dense, external zone. In order to constrain the location of the CH_3OH , we overplot the density and temperature structure derived by CKB2012 on the density-temperature χ^2 contour plot of the LVG analysis. As can be seen from Fig. 3, the density-temperature χ^2 contours intercept the L1544 structure when the source size is between $100''$ and $140''$, namely the CH_3OH emitting gas is at a radius between about 6800 and 9600 AU from the center. At these radii the CKB2012 structure predicts a density of $3\text{--}1.5 \times 10^4 \text{ cm}^{-3}$ and a temperature of ~ 10 K. The very recent work by Bizzocchi et al. 2014 reach the same conclusion.

The coincidence between the CH_3OH emitting region with that where the gaseous water abundance is the largest (see §2) is remarkable. In other words, the LVG analysis strongly suggests that methanol has an enhanced abundance where the FUV photons desorb water molecules. It is, therefore, natural to conclude that methanol has the same origin, namely it is photodesorbed from the icy mantles (Andrade et al. 2010).

The identification of the region where the CH_3OH lines are emitted has an obvious impact on the estimate of the methanol abundance, as, in order to obtain it, one has to divide the measured column density of Tab. 2 by the H_2 column density of the emitting region, namely $\sim 6\text{--}4 \times 10^{21} \text{ cm}^{-2}$, and not the whole L1544 core, which is ~ 30 times larger. Therefore, the (E + A) methanol abundance is $\sim 6 \times 10^{-9}$.

It is natural to assume that the emission from the other detected COMs comes from the same outer layer of L1544, rather than the core itself. The rotational temperatures (≥ 10 K) in Tab. 2 support this hypothesis. Therefore, we computed the COMs abundances following this assumption. The resulting abundances, reported in Tab. 2, vary from $\sim 5 \times 10^{-9}$ for the CH_3CCH , the most abundant COM after methanol, to $\sim 5 \times 10^{-11}$ for C_3O , the least abundant. Finally, the upper limits to the column density of CH_3OCH_3 , HCOOCH_3 and CH_3O convert into an upper limit to their abundance of 2×10^{-10} , 1.5×10^{-9} and 1.5×10^{-10} , respectively.

6. Chemical modeling

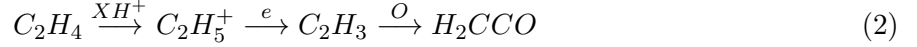
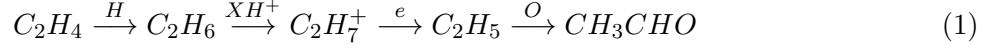
In order to shed light on the formation pathways of the observed COMs, we run a simple chemical model where we first computed the steady state abundances of all the species and then studied the effect on the COMs abundances caused by the injection of grain mantle species into the gas phase. We do not pretend here to describe the situation with a self-consistent model, but just to understand what species from the mantles are needed to reproduce the observed COMs and in what approximate amount. To make things as simple as possible, we considered two species: methanol, known to be present in the mantles, and ethene (C_2H_4). The latter has not been detected in the ices (with an abundance larger than $\sim 10^{-7}$), but it is the first step toward ethane (C_2H_6), whose oxydation leads to acetaldehyde, among other oxygen bearing COMs (Charnley 2004). In addition, we considered the elemental oxygen (in the gas) as a parameter, in order to account for the amount of oxygen trapped into the mantle ices.

We used the Nahoon gas-phase chemical model (<http://kida.obs.u-bordeaux1.fr/models/>; Wakelam et al. 2010), which computes the chemical evolution of species as a function of time for a fixed temperature and density. The chemical network kida.uva.2011 (<http://kida.obs.u-bordeaux1.fr/>) has been updated following Loison et al. (2014) and includes 6680 reactions over 486 species. In our computations we used the following elemental abundances (with respect to H nuclei): He=0.07, C= 5×10^{-5} , N= 2×10^{-5} , Si= 8×10^{-9} , S= 8×10^{-8} , Fe= 3×10^{-9} , Na= 2×10^{-9} , Mg = 7×10^{-9} , Cl= 1×10^{-9} , P= 2×10^{-10} . The oxygen elemental abundance was such to have the following C/O abundance ratios: 0.5, 0.6, 0.7 and 0.8. For the first step, we adopted a gas and dust temperature of 10 K, an H density of $2 \times 10^4 \text{ cm}^{-3}$, a visual extinction of 10 mag and a cosmic rays ionization rate of $3 \times 10^{-17} \text{ s}^{-1}$. We let the chemical composition evolve until steady state is reached. The abundances from this first step were then used as initial abundances for the second step, where we changed the abundance of methanol and ethene separately. In the following, we discuss the results for the detected species.

C_3O is the longest oxygen-bearing carbon chain observed in the interstellar medium (ISM). So far, very few detections of the C_3O have been reported and only one in a cold dark cloud core, TMC-1, unusually carbon-rich (Matthews et al. 1984; Kaifu et al. 2004). Loison et al. (2014) showed that the reactions between carbon chain molecules and radicals (C_n , C_nH , C_nH_2 , $C_{2n+1}O...$) with O atoms produce large enough abundances of the C_3O . We, therefore, started modeling this species as it provides constraints on the amount of gaseous oxygen. We could reproduce the observed C_3O abundance only when the lowest C/O ratio of 0.5 is used, namely when a large fraction of oxygen is in the gas phase. This is in remarkable agreement with the CKB2012 model, which predicts that a large fraction of water is photodesorbed from the grain mantles, making the gas oxygen rich.

CH_3OH is known to be a grain surface product, so that it is no surprising that a pure gas phase model does not reproduce the measured abundance. Injecting $\sim 1 \times 10^{-8}$ methanol from the ices provides the observed amount of methanol. This is a tiny fraction with respect to the methanol formed on the grain surfaces during the prestellar phase (e.g. Taquet et al. 2012).

CH_3CHO and H_2CCO are overabundant with respect to the predictions of the step 1 model, by about three and one orders of magnitude, respectively. However, the injection of ethene with an abundance of 5×10^{-9} is enough to reproduce the measured abundances through the following sequences (Charnley et al. 1992):



CH_3CCH is also overabundant with respect to the predictions of the step 1 model, by about five orders of magnitudes. The injection of 5×10^{-9} ethene increases the abundance by three orders of magnitude but it is still not enough to reproduce the measured abundance. Öberg et al. (2013) suggested that an important formation pathway in cold gas is missing for CH_3CCH in the models, as reinforced by our new measurements.

$t\text{-HCOOH}$ is the only species underabundant with respect to the predicted value of the step 1 model, by about one order of magnitude. This suggests that, in this case, routes of destruction of this species are probably missing.

Finally, the non detection of CH_3OCH_3 , $HCOOCH_3$ and CH_3O is consistent with our and Vasyunin & Herbst (2013) model predictions.

7. Discussion and conclusions

The three major results of this work are:

1. The detection of CH_3OH , CH_3CHO , $t\text{-HCOOH}$, H_2CCO , CH_3CCH , and C_3O . Their abundances are equal to $\sim 1 \times 10^{-11}$ (CH_3CHO and $t\text{-HCOOH}$), $\sim 5 \times 10^{-11}$ (C_3O), $\sim 1 \times 10^{-12}$ (H_2CCO), $\sim 5 \times 10^{-9}$ (CH_3CCH), and $\sim 6 \times 10^{-9}$ (CH_3OH). No other oxygen bearing COM has been detected, including CH_3OCH_3 , $HCOOCH_3$ and CH_3O , species that have been detected in other prestellar cores (§1). The upper limit to their abundances is $\leq 10^{-9} - 10^{-10}$.
2. The gas has to be oxygen rich ($C/O \sim 0.5$) and an injection of a relatively small amount of methanol ($\sim 10^{-8}$) and ethene ($\sim 5 \times 10^{-9}$) from the ices is enough to reproduce the observed abundances of CH_3OH , CH_3CHO , H_2CCO , and C_3O . On the contrary, the model overestimates the abundance of $t\text{-HCOOH}$ and underestimates that of CH_3CCH .
3. Probably, the most important result is the discovery that the CH_3OH emission comes from the border of the L1544 core, at ~ 8000 AU, in a region where the ices are desorbed through non-thermal processes. We suggest that very likely also the other detected COMs have the same origin. The large rotational temperatures support this hypothesis.

L1544 is the third prestellar core, after B1-b and L1689B, where COMs have been detected (Öberg et al. 2010; Cernicharo et al. 2012; Bacmann et al. 2012). In the three cores, acetaldehyde, ketene and acid formic have similar column densities (within a factor 3–4). The same applies to methanol in L1544 and B1-b. Finally, also the column densities of methyl formate and dimethyl ether are similar in B1-b and L1689B, and consistent with our upper limits. This may lead to suppose that also in B1-b and L1689B the observed COM line emission originates in an outer layer where desorption is not fully compensated by the freeze-out rather than in the core. If this is the case, the COMs chemistry in prestellar cores may be driven by the non-thermal desorption of simple ice components, namely hydrogenated species like methanol and ethene, and not necessarily by other processes (e.g. Cernicharo et al. 2012; Vasyunin & Herbst 2013).

In conclusion, L1544 is a core on the verge of collapsing (Caselli et al. 2002; Keto et al. 2014). The center of the core is very cold and dense, and all species are largely frozen onto the grain mantles (CKB2012). There is, however, a region, at ~ 8000 AU from the center, where FUV photons (the product of the interaction of the cosmic rays with the H_2 molecules according to CKB2012) photodesorb a tiny fraction of the frozen water and possibly methanol and ethene. These molecules react with other species in the gas phase and produce a detectable amount of acetaldehyde, ketene and tricarbon monoxide. It is possible, but not demonstrated, that a similar situation occurs also in other prestellar cores, for example in B1-b and L1689B, where previous observations have detected COMs with similar column densities. If this is the case, the quoted abundances may need some revision. Also in these cases, the COMs chemistry may be driven by the desorption of simple hydrogenated species from the ices. Higher spatial resolution observations are necessary to settle the issue and better constrain the formation routes of COMs in prestellar cores.

We thank P. Caselli, J.-C. Loison and M. Ruaud for helpful discussion.

Facilities: IRAM, CASSIS.

REFERENCES

- Andrade D. P. P., Rocco M. L. M., Boechat-Roberty H. M. 2010, MNRAS, 409, 1289
- Bacmann A., Taquet V., Faure A., Kahane C., Ceccarelli C. 2012, A&A, 541 12
- Bizzocchi, L., Caselli, P., Spezzano, S., Leonardo, E., arXiv:1408.2491
- Blake G. A., Sutton E. C., Masson C. R., Phillips T. G. 1987, ApJ, 315, 621
- Bottinelli S., Ceccarelli C., Lefloch B. et al. 2004, ApJ, 615, 354
- Cazaux S., Tielens A. G. G. M., Ceccarelli C., Castets A., Wakelam V. et al. 2003, ApJ, 593, 51

- Caselli P., Walmsley C. M., Zucconi A. et al. 2002, ApJ, 565, 331
- Caselli P., van der Tak, F. F. S., Ceccarelli, C., Bacmann, A., 2003, A&A, 403, 37
- Caselli, P., Keto, E., Bergin, E. A. et al. 2012, ApJ, 109, 301: CKB2012
- Caselli, P. & Ceccarelli C. 2012, A&A Rev., 20, 56
- Ceccarelli, C., Maret, S., Tielens, A. G. G. M., Castets, A., & Caux, E. 2003, A&A, 410, 587
- Ceccarelli C. 2005, in *Astrochemistry: Recent Successes and Current Challenges*, Eds. Lis D. C., Blake G. A., Herbst E., Cambridge University Press, p. 1
- Cernicharo J., Marcelino N., Roueff E. et al. 2012, ApJ, 759, 43
- Charnley S. B. 2004, Ad.Sp.Res., 33, 23
- Crapsi A., Caselli P., Walmsley M., Myers P. C., Tafalla M. 2005, ApJ, 619, 379
- Crapsi A., Caselli P., Walmsley M. et al. 2007, ApJ, 470, 221
- Cummins S. E., Linke R. A., Thaddeus P. 1986, ApJS, 60, 819
- Jaber A., Ceccarelli C., Kahane C., Caux E. 2014, ApJ, in press
- Dominik C., Ceccarelli C., Hollenbach D., Kaufmann M. 2005, ApJ, 635, L85
- Dubernet M.-L., Alexander M. H., Ba Y. A. et al. 2013, A&A, 553, 50
- Garrod R.T. & Herbst E., 2006, A&A, 457, 927
- Garrod R.T., Vasyunin A. I., Semenov D. A., Wiebe D. S., & Henning T. 2009, ApJ, 700, L43
- Herbst E., van Dishoeck E. F. 2009, ARA&A, 47, 427
- Hollenbach D., Kaufman M. J., Bergin E. A., Melnick G. J. 2009, ApJ, 690, 1497
- Kaifu N., Ohishi M., Kawaguchi K. et al. 2004, PASJ, 56, 69
- Keto E., Rawlings J., Caselli P. 2014, MNRAS, 440, 2616, 301
- Loison J.-C., Wakelam V., Hickson K., Bergeat, A. Mereau, R. 2014, MNRAS, 437, 930
- Matthews H. E., Irvine W. M., Friberg P., Brown R. D., Godfrey P. D., 1984, Nature, 310, 125
- Öberg K. I., Bottinelli S., Jørgensen J. K., van Dishoeck E. F. 2010, ApJ, 716, 825
- Öberg K. I., Boamah M. D., Fayolle E. C. et al. 2013, ApJ, 771, 95
- Rabli D. & Flower D. 2010, MNRAS, 2010 406, 95

- Requena-Torres M. A., Martin-Pintado J., Rodriguez-Franco A., et al. 2006, A&A, 455, 971
- Taquet, V., Ceccarelli, C., & Kahane, C. 2012, A&A, 538, A42
- Vasyunin, A. I., & Herbst, E. 2013, ApJ, 769, 34
- Vastel C., Caselli P., Ceccarelli C. et al. 2006, ApJ, 645, 1198
- Wakelam V., Herbst E., Le Boulbot J. et al. 2010, A&A, 517, 21

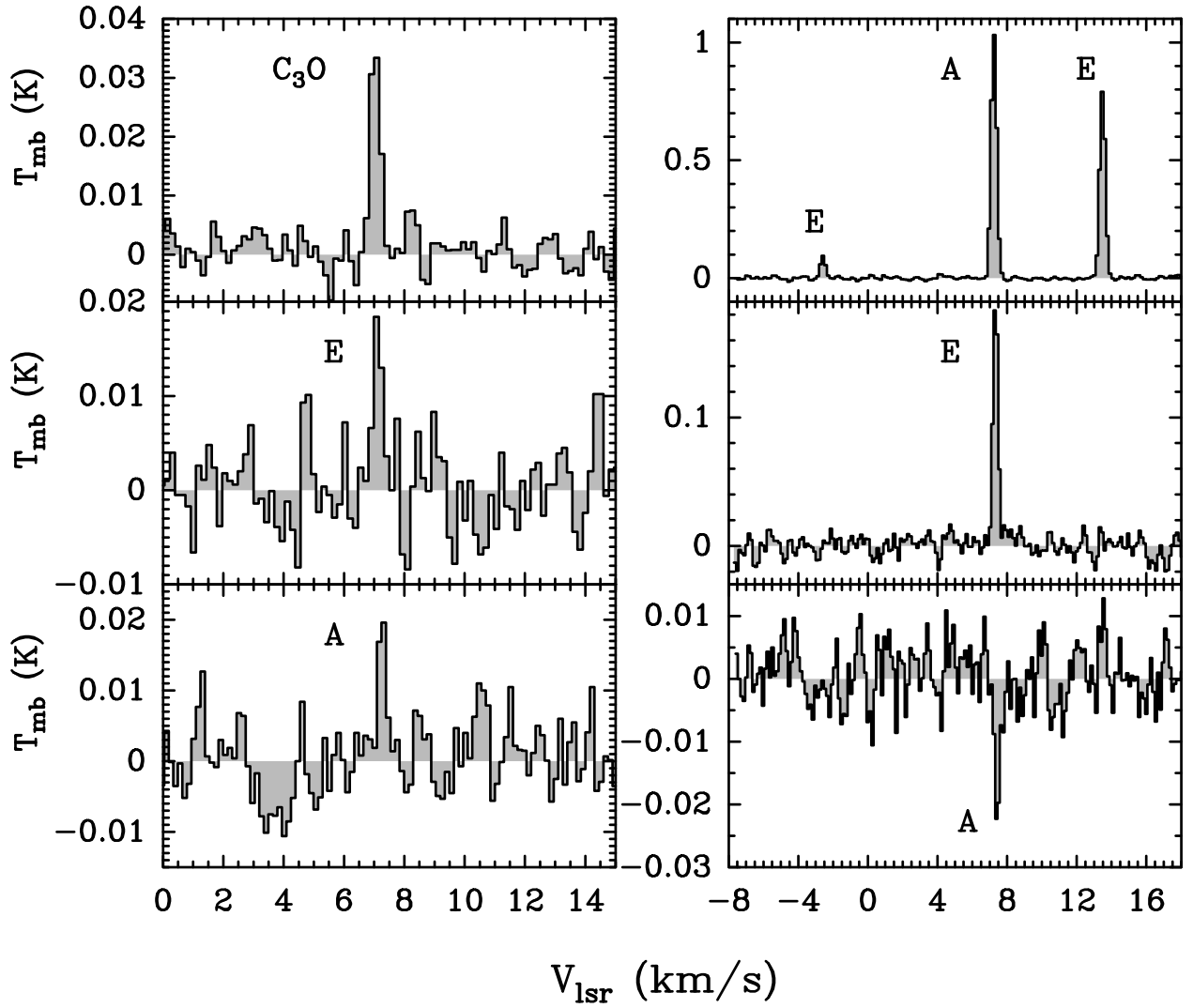


Fig. 1.— Spectra of the detected lines from C_3O (upper left pannel) and CH_3OH (the other panels). The temperatures are main beam temperatures.

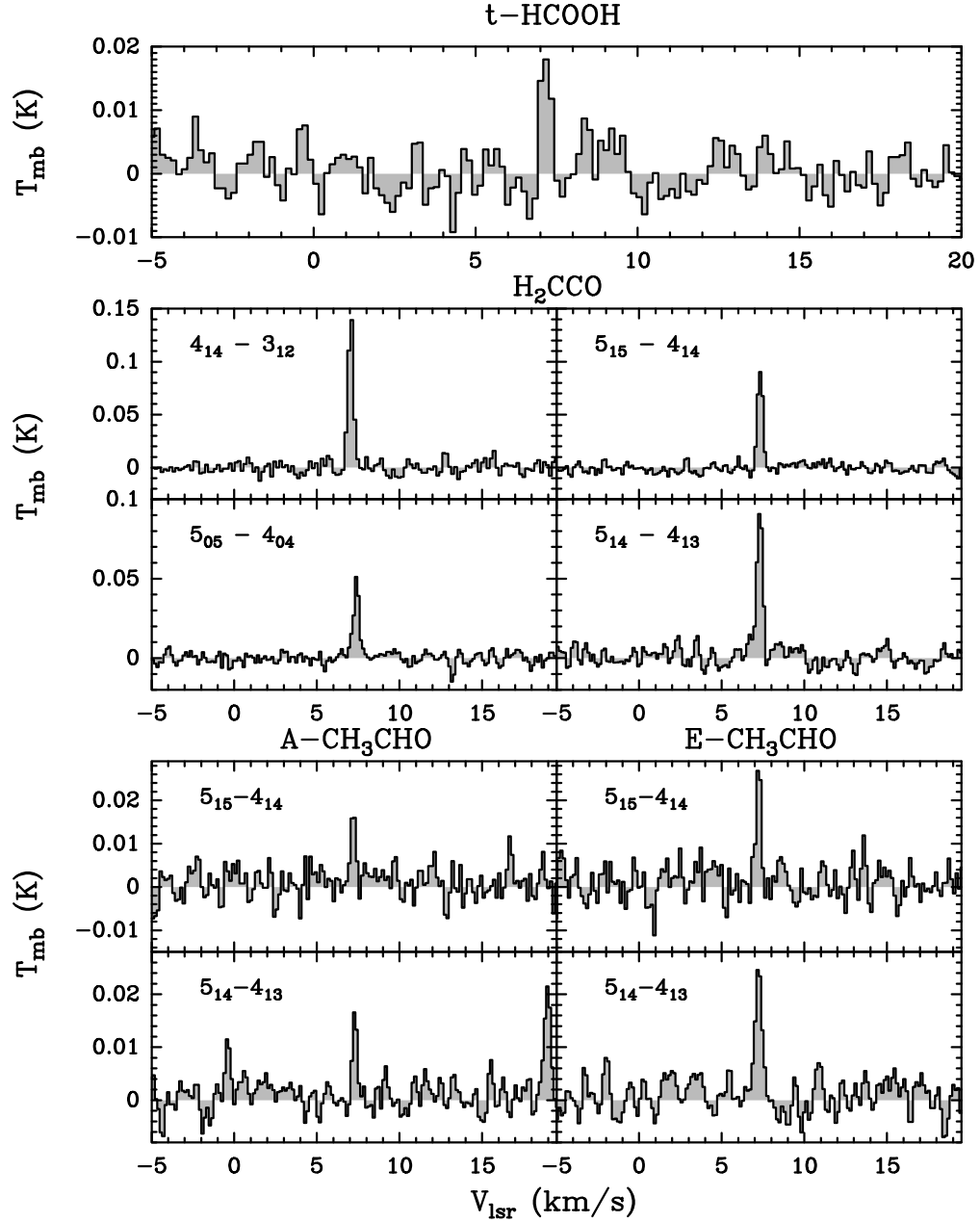


Fig. 2.— Spectra of the detected lines from $t\text{-HCOOH}$ (top panel), H_2CCO (central panel) and CH_3CHO (bottom panel). The temperatures are main beam temperatures.

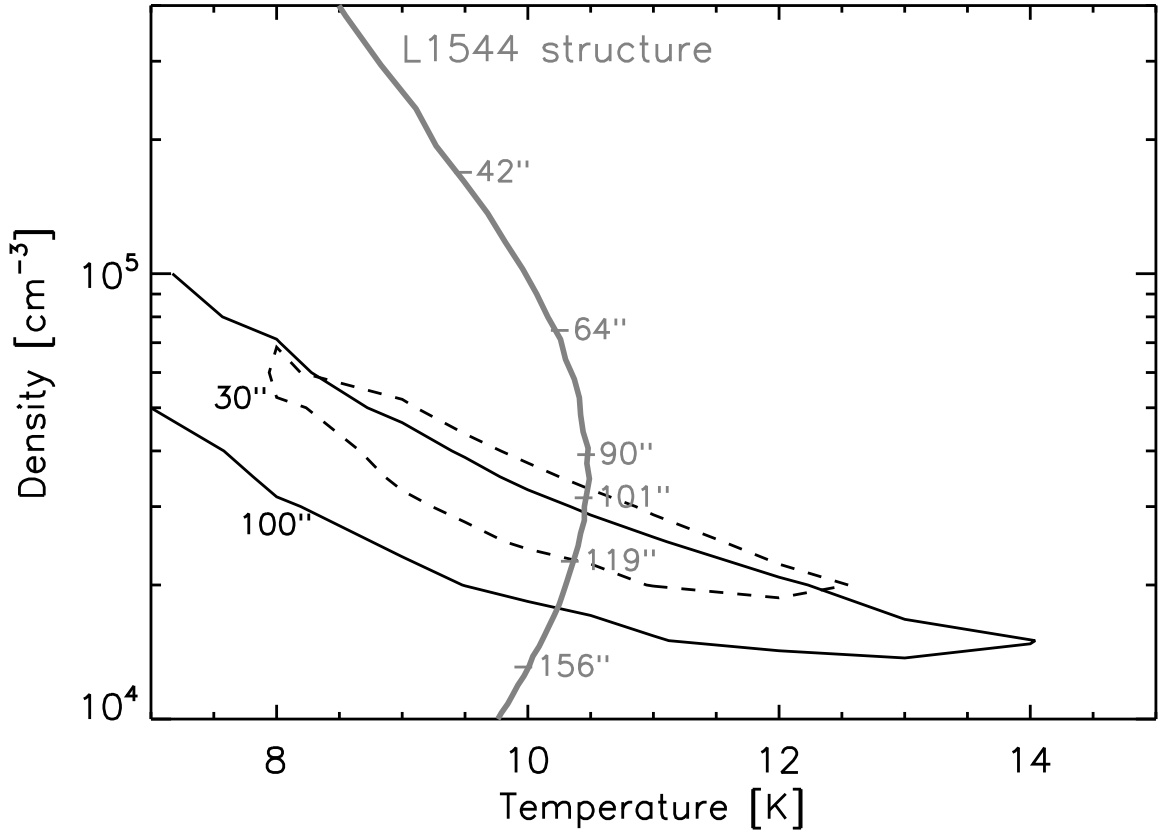


Fig. 3.— Results from the LVG analysis of the CH_3OH lines. The black lines show the $\chi^2=0.8$ contour plot for $N(\text{CH}_3\text{OH})=3.8 \times 10^{13} \text{ cm}^{-2}$ and a size of 30'' (dashed) and $N(\text{CH}_3\text{OH})=2.6 \times 10^{13} \text{ cm}^{-2}$ and size 100'' (solid), the two extremes of the solutions with reduced $\chi^2 \leq 0.8$. The grey line shows the densities and temperatures at different distances from the center (diameter in arcsec are marked along the curve) predicted for the structure of L1544 by CKB2012.

Table 1. Spectroscopic parameters of C₃O and the COMs detected toward L1544 and results from the line Gaussian fits. The rms on a 50 kHz frequency bin was computed over a range of 40 km/s. The error in the main-beam temperature T_{mb} does not include the calibration. Note that the A and E forms for CH₃OH are taken from the CASSIS database. The line labelled ^a is in absorption.

Species	Database	QN	Frequency (GHz)	E _{up} (K)	A _{ij} (s ⁻¹)	rms (mK)	T _{mb} (mK)	FWHM (km s ⁻¹)	V _{LSR} (km s ⁻¹)
C ₃ O	52501	9 – 8	86.59368	20.78	2.05×10^{-5}	3.5	36.8 ± 3.5	0.39 ± 0.04	7.04 ± 0.02
		10 – 9	96.21462	25.40	2.82×10^{-5}	6.1
		11 – 10	105.83536	30.48	3.77×10^{-5}	4.9
A-CH ₃ CHO	44003	515-414	93.58091	15.75	2.53×10^{-5}	3.5	17.8 ± 3.4	0.33 ± 0.07	7.20 ± 0.03
		505-404	95.96346	13.84	2.84×10^{-5}	5.9	25.6 ± 3.6	0.81 ± 0.13	7.35 ± 0.06
		514-413	98.90094	16.51	2.99×10^{-5}	2.7	17.2 ± 2.6	0.31 ± 0.05	7.30 ± 0.02
E-CH ₃ CHO	44003	515-414	93.59523	15.82	2.53×10^{-5}	3.9	29.3 ± 3.8	0.33 ± 0.05	7.23 ± 0.02
		505-404	95.94744	13.93	2.84×10^{-5}	5.8	50.5 ± 8.4	0.24 ± 0.05	7.20 ± 0.01
		514-413	98.86331	16.59	2.99×10^{-5}	3.2	24.7 ± 2.4	0.49 ± 0.05	7.23 ± 0.02
t-HCOOH	46506	414-313	86.54619	13.57	6.35×10^{-6}	3.4	19.9 ± 3.3	0.34 ± 0.07	7.17 ± 0.03
H ₂ CCO	42501	413-312	81.58623	22.84	5.33×10^{-6}	5.8	147.2 ± 5.6	0.38 ± 0.02	7.05 ± 0.01
		515-414	100.09451	27.46	1.03×10^{-5}	4.2	95.5 ± 3.7	0.39 ± 0.02	7.32 ± 0.01
		505-404	101.03663	14.55	1.10×10^{-5}	3.5	49.1 ± 3.0	0.42 ± 0.03	7.39 ± 0.01
		514-413	101.98143	27.74	1.09×10^{-5}	5.3	95.3 ± 4.5	0.41 ± 0.02	7.30 ± 0.01
E-CH ₃ CCH	40592	52-42	85.45077	41.21	1.70×10^{-6}	3.8	70.8 ± 3.4	0.46 ± 0.03	7.18 ± 0.01
		51-41	85.45567	19.53	1.95×10^{-6}	3.6	740.8 ± 15.9	0.43 ± 0.01	7.18 ± 0.01
		50-40	85.45730	12.30	2.03×10^{-6}	3.6	740.2 ± 10.3	0.46 ± 0.01	7.18 ± 0.01
		62-52	102.54014	46.13	3.16×10^{-6}	4.4	61.1 ± 3.5	0.46 ± 0.03	7.40 ± 0.01
		61-51	102.54602	24.45	3.46×10^{-6}	4.4	612.6 ± 10.6	0.47 ± 0.01	7.38 ± 0.01
		60-50	102.54798	17.23	3.56×10^{-6}	4.5	632.4 ± 10.8	0.47 ± 0.01	7.38 ± 0.01
E-CH ₃ OH	32083	5 -1 0 - 4 0 0	84.52117	32.49	1.97×10^{-6}	4.1	18.9 ± 4.0	0.37 ± 0.09	7.12 ± 0.04
		2 -1 0 - 1 -1 0	96.73936	4.64	2.55×10^{-6}	6.8	805.0 ± 6.0	0.38 ± 0.01	7.24 ± 0.01
		2 0 0 - 1 0 0	96.74454	12.19	3.40×10^{-6}	6.1	95.8 ± 5.7	0.34 ± 0.02	7.25 ± 0.01
		0 0 0 - 1 -1 0	108.89394	5.23	1.47×10^{-5}	8.1	195.2 ± 7.1	0.34 ± 0.01	7.33 ± 0.01
E- ¹³ CH ₃ OH	32502	2 -1 0 - 1 -1 0	94.40516	4.53	2.38×10^{-6}	6.8	20.1 ± 6.0	0.45 ± 0.15	7.02 ± 0.06
A-CH ₃ OH	32093	2 0 + 0 - 1 0 + 0	96.74137	6.97	3.40×10^{-6}	6.6	1047.5 ± 6.1	0.39 ± 0.01	7.24 ± 0.01
		2 1 - 0 - 1 1 - 0	97.58280	21.56	2.62×10^{-6}	5.6	21.8 ± 5.7	0.29 ± 0.09	7.27 ± 0.04
		3 1 + 0 - 4 0 + 0	107.01383	28.35	3.06×10^{-6}	4.4	22.3 ± 3.5^a	0.41 ± 0.08	7.45 ± 0.03
A- ¹³ CH ₃ OH	32502	2 0 + 0 - 1 0 + 0	94.40713	6.80	3.17×10^{-6}	6.6	25.9 ± 6.1	0.40 ± 0.15	7.23 ± 0.05

Table 2. Column densities and abundances of COMs in L1544. Notes: a) LTE minimisation procedure; b) assumed $T_{ex}=10$ K; c) non-LTE LVG analysis (see text). The abundances x have been computed assuming $N(H_2)=5 \times 10^{21} \text{ cm}^{-2}$. The final error on the column densities and abundances is about a factor 2.

Species	T_{ex} (K)	T_k (K)	n_{H_2} (cm^{-3})	N (cm^{-2})	x
C_3O^b	10			2×10^{11}	5×10^{-11}
CH_3CHO^a	17 ± 1			5×10^{11}	1×10^{-10}
$t\text{-HCOOH}^b$	10			5×10^{11}	1×10^{-10}
H_2CCO^a	27 ± 1			5×10^{12}	1×10^{-9}
$E\text{-}CH_3CCH^a$	11 ± 2			2×10^{13}	5×10^{-9}
CH_3OH^c		10	3×10^4	3×10^{13}	6×10^{-9}
$CH_3OCH_3^b$	10			$\leq 1 \times 10^{12}$	$\leq 2 \times 10^{-10}$
$HCOOCH_3^b$	10			$\leq 6 \times 10^{12}$	$\leq 1.5 \times 10^{-9}$
CH_3O^b	10			$\leq 6 \times 10^{11}$	$\leq 1.5 \times 10^{-10}$